

Nonlocal edge state transport in the quantum spin Hall state

Andreas Roth,¹ Christoph Brüne,¹ Hartmut Buhmann,¹ Laurens W. Molenkamp,^{1*}
Joseph Maciejko,² Xiao-Liang Qi,² Shou-Cheng Zhang²

¹Physikalisches Institut (EP3) and Röntgen Center for Complex Material Systems,
Universität Würzburg, Am Hubland, 97074 Würzburg, Germany

²Department of Physics, Stanford University, Stanford, CA 94305, USA

*To whom correspondence should be addressed; E-mail: molenkmp@physik.uni-wuerzburg.de.

We present direct experimental evidence for nonlocal transport in HgTe quantum wells in the quantum spin Hall regime, in the absence of any external magnetic field. The data conclusively show that the non-dissipative quantum transport occurs through edge channels, while the contacts lead to equilibration between the counter-propagating spin states at the edge. We show that the experimental data agree quantitatively with the theory of the quantum spin Hall effect.

The quantum spin Hall (QSH) state (1, 2) is a topologically nontrivial state of matter which exists in the absence of any external magnetic field. It has a bulk energy gap but gapless helical edge states protected by time reversal symmetry. In the QSH regime, opposite spin states forming a Kramers doublet counter-propagate at the edge (3, 4). Recently, the QSH state has been theoretically predicted in HgTe quantum wells (5). There is a topological quantum phase transition at a critical thickness d_c of the quantum well, separating the trivial insulator state for $d < d_c$ from the QSH insulator state for $d > d_c$. Soon after the theoretical prediction, evidence

for the QSH state has been observed in transport measurements (6). In the QSH regime, experiments measure a conductance close to $2e^2/h$, which is consistent with quantum transport due to helical edge states. However, such a conductance quantization in small Hall bars does not allow us to distinguish experimentally between ballistic and edge channel transport in a convincing manner. Thus it is of the utmost importance for this field to be able to prove experimentally in an unambiguous manner the existence of edge channels in HgTe quantum wells.

In conventional diffusive electronics, bulk transport satisfies Ohm's law. The resistance is proportional to the length and inversely proportional to the cross-sectional area, implying the existence of a local resistivity or conductivity tensor. However, the existence of edge states necessarily leads to nonlocal transport which invalidates the concept of local resistivity. Such nonlocal transport has been experimentally observed in the quantum Hall (QH) regime in the presence of a large magnetic field (7), and the nonlocal transport is well described by a quantum transport theory based on the Landauer-Büttiker formalism (8). These measurements are now widely acknowledged as constituting definitive experimental evidence for the existence of edge states in the QH regime.

In this work, we report nonlocal transport measurements in HgTe quantum wells that unequivocally demonstrate the existence of extended edge channels. We have fabricated more complicated structures compared to a standard Hall bar that allow a detailed investigation of the transport mechanism. The data present the first definitive evidence for the actual occurrence of helical edge channels in our samples. In addition, we present the theory of quantum transport in the QSH regime, and uncover the remarkable effects of macroscopic time irreversibility on the helical edge states.

We present experimental results on four different devices, with layouts as outlined below. The behavior in these structures is exemplary for the around 50 devices we studied. The devices are fabricated from HgTe/(Hg,Cd)Te quantum well (QW) structures with well thicknesses

of $d = 7.5$ nm (samples S1, S2 and S3) and 9.0 nm (sample S4). Note that all wells have a thickness $d > d_c \simeq 6.3$ nm, and thus exhibit the topologically non-trivial inverted band structure. At zero gate voltage, the samples are n-type and have a carrier density of about $n_s = 3 \times 10^{11}$ cm⁻² and a mobility of 1.5×10^5 cm²/(Vs), with small variations between the different wafers. The actual devices are lithographically patterned using electron-beam lithography and subsequent Ar ion-beam etching. Devices S1 and S2 are micron-scale Hall bars with exact dimensions as indicated in the insets of Fig. 1. S3 and S4 are dedicated structures for identifying non-local transport, schematic structure layouts are given in Fig. 2. All devices are fitted with a 110-nm-thick Si₃N₄/SiO₂ multilayer gate insulator and a 5/50 nm Ti/Au gate electrode stack. By applying a voltage V_g to the top gate the electron carrier density of the QW can be adjusted, going from an n-type behavior at positive gate voltages through the bulk insulator state into a p-type regime at negative gate voltages. For reasons of comparison, the experimental data in Figs. 1,3, and 4 are plotted as a function of a normalized gate voltage $V^* = V_g - V_{thr}$ (V_{thr} is defined as the voltage for which the resistance is largest). Measurements are performed at a lattice temperature of 10 mK using low-frequency (13 Hz) lock-in techniques under voltage bias. The two terminal and four terminal conductance results are shown in Fig. 1. The four terminal resistance shows a maximum at about $h/2e^2$, in agreement with the results of Ref. (6). We also study the two terminal resistance. The contact resistance should be insensitive to the gate voltage, and can be measured from the resistance deep in the metallic region. By subtracting the contact resistance we find that the two terminal resistance has its maximum of about $3h/2e^2$. As we shall see in the following discussions, this value is exactly what is expected from the theory of QSH edge transport obtained from the Landauer-Büttiker formula.

We now present the theory of quantum transport due to the helical edge states in the QSH regime. Within the general Landauer-Büttiker formalism (9), the current-voltage relationship is

expressed as

$$I_i = \frac{e^2}{h} \sum_j (T_{ji} V_i - T_{ij} V_j), \quad (1)$$

where I_i is the current flowing out of the i -th electrode into the sample region, V_i is the voltage on the i -th electrode, and T_{ji} is the transmission probability from the i -th to the j -th electrode. The total current is conserved in the sense that $\sum_i I_i = 0$. A voltage lead j is defined by the condition that it draws no net current, *i.e.* $I_j = 0$. The physical currents are left invariant if the voltages on all electrodes are shifted by a constant amount μ , implying that $\sum_i T_{ij} = \sum_i T_{ji}$. In a time-reversal invariant system, the transmission coefficients satisfy the condition $T_{ij} = T_{ji}$.

For a general two-dimensional sample, the number of transmission channels scales with the width of the sample, so that the transmission matrix T_{ij} is complicated and non-universal. However, a tremendous simplification arises if the quantum transport is entirely dominated by the edge states. In the QH regime, chiral edge states are responsible for the transport. For a standard Hall bar with N current and voltage leads attached (cf. the insets of Fig. 1 with $N = 6$), the transmission matrix elements for the $\nu = 1$ QH state are given by $T(\text{QH})_{i+1,i} = 1$, for $i = 1, \dots, N$, and all other matrix elements vanish identically. Here we periodically identify the $i = N + 1$ electrode with $i = 1$. Chiral edge states are protected from backscattering, therefore, the i -th electrode transmits perfectly to the neighboring $(i + 1)$ th electrode on one side only. In the example of current leads on the electrodes 1 and 4, and voltage leads on the electrodes 2, 3, 5 and 6, one finds that $I_1 = -I_4 \equiv I_{14}$, $V_2 - V_3 = 0$ and $V_1 - V_4 = \frac{h}{e^2} I_{14}$, giving a four-terminal resistance of $R_{14,23} = 0$ and a two-terminal resistance of $R_{14,14} = \frac{h}{e^2}$.

In the case of helical edge states in the QSH regime, opposite spin states form a Kramers pair, counter-propagating on the same edge. The helical edge states are protected from backscattering due to time reversal symmetry, and the transmission from one electrode to the next is perfect. From this point of view, the helical edge states can be viewed as two copies of chiral edge states related by time reversal symmetry. Therefore, the transmission matrix is given by

$T(\text{QSH}) = T(\text{QH}) + T^\dagger(\text{QH})$, implying that the only non-vanishing matrix elements are given by

$$T(\text{QSH})_{i+1,i} = T(\text{QSH})_{i,i+1} = 1, \quad (2)$$

Considering again the example of current leads on the electrodes 1 and 4, and voltage leads on the electrodes 2, 3, 5 and 6, one finds that $I_1 = -I_4 \equiv I_{14}$, $V_2 - V_3 = \frac{h}{2e^2} I_{14}$ and $V_1 - V_4 = \frac{3h}{e^2} I_{14}$, giving a four-terminal resistance of $R_{14,23} = \frac{h}{2e^2}$ and a two-terminal resistance of $R_{14,14} = \frac{3h}{2e^2}$. The experimental data in Fig. 1 neatly confirm this picture. For both micro Hall-bar structures S1 and S2, that differ only in the dimensions of the area between the voltage contacts 3 and 4 we observe exactly the expected resistance values for $R_{14,23} = \frac{h}{2e^2}$ and $R_{14,14} = \frac{3h}{2e^2}$ for gate voltages where the samples are in the QSH regime.

Conceptually, one might sense a paradox between the dissipationless nature of the QSH edge states and the finite four-terminal longitudinal resistance $R_{14,23}$, which vanishes for the QH state. We can generally assume that the microscopic Hamiltonian governing the voltage leads is invariant under time reversal symmetry, therefore, one would naturally ask how such leads could cause the dissipation of the helical edge states, which are protected by time reversal symmetry? In nature, the time reversal symmetry can be broken in two ways, either at the level of the microscopic Hamiltonian, or at the level of the macroscopic irreversibility in systems whose microscopic Hamiltonian respects the time reversal symmetry. When the helical edge states propagate without dissipation inside the QSH insulator between the electrodes, neither forms of time reversal symmetry breaking are present. As a result, the two counter-propagating channels can be maintained at two different quasi chemical potentials, leading to a net current flow. However, once they enter the voltage leads, they interact with a reservoir containing infinitely many low-energy degrees of freedom, and the time reversal symmetry is effectively broken by the macroscopic irreversibility. As a result, the two counter-propagating channels equilibrate at the same chemical potential, determined by the voltage of the lead. Dissipation

occurs with the equilibration process. The transport equation (1) breaks the macroscopic time reversal symmetry, even though the microscopic time reversal symmetry is ensured by the relationship $T_{ij} = T_{ji}$. In contrast to the case of QH state, the absence of dissipation of the QSH helical edge states is protected by Kramers' theorem, which relies on the quantum phase coherence of wavefunctions. Thus dissipation can occur once the phase coherence is destroyed in the metallic leads. On the contrary, the robustness of QH chiral edge states does not require phase coherence. A more rigorous and microscopic analysis on the different role played by a metallic lead in QH and QSH states is provided in the supporting online text, the result of which agrees with the simple transport equation (1) and (2). These two equations correctly describe the dissipationless quantum transport inside the QSH insulator, and the dissipation inside the electrodes. One can subject these two equations to more stringent experimental tests than the two-and four-terminal experiments of Fig. 1 by considering devices S3 and S4, as depicted in Fig. 2.

A further difference between helical and chiral edge channels is evident from our experiments on the six-terminal device S3, as shown in Fig. 3. When the longitudinal resistance of device S3 is measured by passing a current through contacts 1 and 4 and by detecting the voltage between contacts 2 and 3 ($R_{14,23}$) [Fig. 1a)], we find, similarly to the results of Fig. 1, the celebrated resistance value of $h/2e^2$ when the bulk of the device is gated into the insulating regime [Fig. 3 a)]. However, the longitudinal resistance is significantly different in a slightly modified configuration, where the current is passed through contacts 1 and 3 and the voltage is measured between contacts 4 and 5 ($R_{13,45}$) [Fig. 3 b)]. We now find $R_{13,45} \approx 8.6 \text{ k}\Omega$, which is markedly different from what one would expect for either the QH transport, or the purely diffusive transport, where this configuration would be equivalent to the previous. Application of equations (1) and (2) actually predicts indeed that the observed behavior is what one expects for helical edge channels. One easily finds that this resistance value can again be expressed

as an integer fraction of the inverse conductance quanta e^2/h : $R_{13,45} = 1/3 h/e^2$. This result shows that the current through the device is influenced by the number of ohmic contacts in the current path. As discussed earlier, these ohmic contacts lead to the equilibration of the chemical potentials between the two counter-propagating helical edge channels inside the contact. There are also some devices for which the maximal resistance does not match the theoretical value obtained from Eqs. (1) and (2), but still remains an integer fraction of the quantum h/e^2 . This result can be naturally understood as due to inhomogeneities in the gate action, e.g. due to interface trap states, inducing some metallic droplets close to the edge channels while the bulk of the sample is insulating. A metallic droplet can cause dephasing of the electronic wave function, leading to fluctuations in the device resistance. For full dephasing, the droplet plays the role of an additional Ohmic contact, just as for the chiral edge channels in the QH regime (7). More details on the effects of additional Ohmic contacts in the QSH state are given in the supporting online text.

Another measurement that directly confirms the non-local character of the helical edge channel transport in the QSH regime is in Fig. 4, which shows data obtained from device S4, in the shape of the letter “H”. In this 4-terminal device the current is passed through contacts 1 and 4 and the voltage is measured between contacts 2 and 3. In the metallic n-type regime (low gate voltage) the voltage signal tends to zero. In the insulating regime, however, the nonlocal resistance signal increases to $\approx 6.5 \text{ k}\Omega$, which again fits perfectly to the result of Landauer-Büttiker considerations: $R_{14,23} = h/4e^2 \approx 6.45 \text{ k}\Omega$. Classically, one would expect only a minimal signal in this configuration (from Poisson’s equation, assuming diffusive transport, one estimates a signal of about $40 \text{ }\Omega$), and certainly not one that increases so strongly when the bulk of the sample is depleted. This signal measured here is fully non-local, and can be taken (as was done twenty years ago for the QH regime) as definite evidence of the existence of edge channel transport in the QSH regime. A similar non-local voltage has been studied in a metallic spin Hall system

with the same H-bar geometry (10), in which case the nonlocal voltage can be understood as a combination of the spin Hall effect and the inverse spin Hall effect (11). The quantized nonlocal resistance $h/4e^2$ we find here is the quantum counterpart of the metallic case. Assuming for example that the chemical potential in contact 1 is higher than that in contact 4 (cf. the layout of S4 in Fig. 2 (b)), more electrons will be injected into the upper edge state in the horizontal segment of the H-bar than into the lower edge state. Since on opposite edges, the right-propagating edge states have opposite spin, this implies that a spin-polarized current is generated by an applied bias $V_1 - V_4$, comparable to a spin Hall effect. When this spin-polarized current is injected into the right leg of the device, the inverse effect occurs. Electrons in the upper edge flow to contact 2 while those in the lower edge will flow to contact 3, establishing a voltage difference between those two contacts due to the charge imbalance between the edges. The right leg of the device thus acts as a detector for the injected spin-polarized current, which corresponds to the inverse spin Hall effect.

In conclusion, we have shown multi-terminal and non-local transport experiments on HgTe microstructures in the QSH regime that unequivocally demonstrate that charge transport occurs through extended helical edge channels. We have extended the Landauer-Büttiker model for multi-terminal transport in the QH regime to the case of helical QSH edge channels, and have shown that this model convincingly explains our observations. These results constitute decisive evidence that the conductance quantization observed in Ref. (6) stems from QSH edge channel transport, which may be used for non-dissipative transfer of information.

References and Notes

1. C. L. Kane, E. J. Mele, *Phys. Rev. Lett.* **95**, 226801 (2005).
2. B.A. Bernevig, S.C. Zhang, *Phys. Rev. Lett.* **96**, 106802 (2006).

3. C. J. Wu, B. A. Bernevig, S. C. Zhang, *Phys. Rev. Lett.* **96**, 106401 (2006).
4. C. Xu, J. Moore, *Phys. Rev. B* **73**, 045322 (2006).
5. B. A. Bernevig, T. L. Hughes, S.C. Zhang, *Science* **314**, 1757 (2006).
6. M. König, *et al.*, *Science* **318**, 766 (2007).
7. C. W. J. Beenakker, H. van Houten, *Solid State Phys.* **44**, 1 (1991).
8. M. Büttiker, *Phys. Rev. B* **38**, 9375 (1988).
9. M. Büttiker, *Phys. Rev. Lett.* **57**, 1761 (1986).
10. C. Brüne, *et al.*, *e-print arXiv: 0812.3768* (2008).
11. E. M. Hankiewicz, L. W. Molenkamp, T. Jungwirth, J. Sinova, *Phys. Rev. B* **70**, 241301(R) (2004).
12. We thank T. Beringer, N. Eikenberg, M. König and S. Wiedmann for assistance in some of the experiments. We gratefully acknowledge financial support by the Deutsche Forschungsgemeinschaft (SFB 410), the German-Israeli Foundation (I-881-138.7/2005), the NSF (grant DMR-0342832), the U.S. Department of Energy, Office of Basic Energy Sciences, under contract DE-AC03-76SF00515, the Focus Center Research Program (FCRP) Center on Functional Engineered Nanoarchitectonics (FENA), the National Science and Engineering Research Council (NSERC) of Canada, and the Stanford Graduate Fellowship Program (SGF). Computational work was made possible by the facilities of the Shared Hierarchical Academic Research Computing Network (SHARCNET:www.sharcnet.ca).

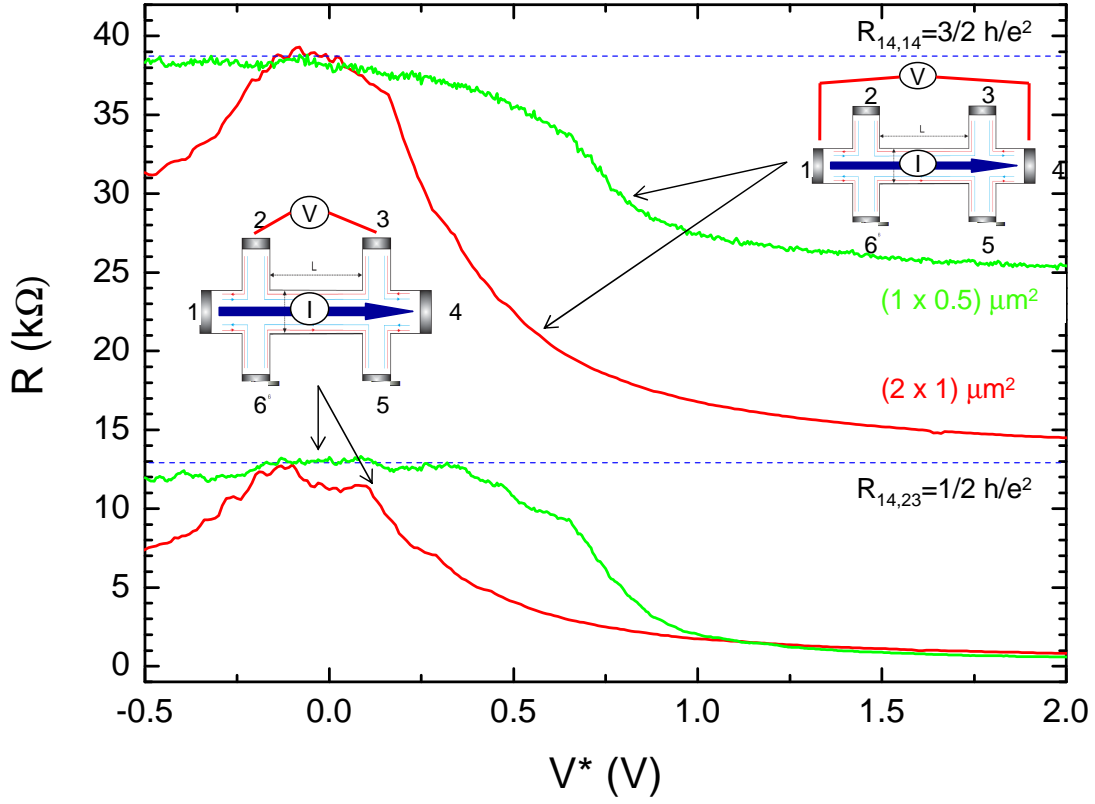


Fig. 1. Two-terminal ($R_{14,14}$) and four-terminal ($R_{14,23}$) resistance versus (normalized) gate voltage for the Hall bar devices S1 and S2 with dimensions as shown in the insets. The dotted blue lines indicate the resistance values expected from the Landauer-Büttiker approach.

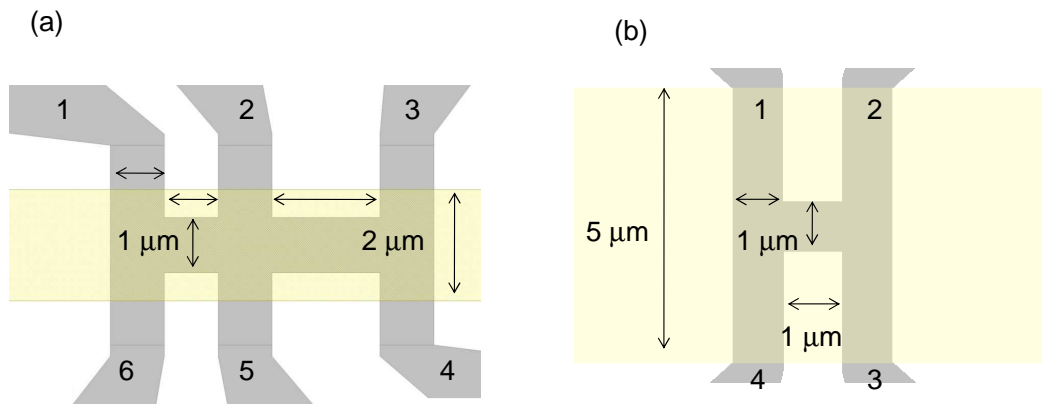


Fig. 2. Schematic layout of devices S3 (a) and S4 (b). The grey areas are the mesa's, the yellow areas the gates, with dimensions as indicated in the figure. The numbers indicate the coding of the leads.

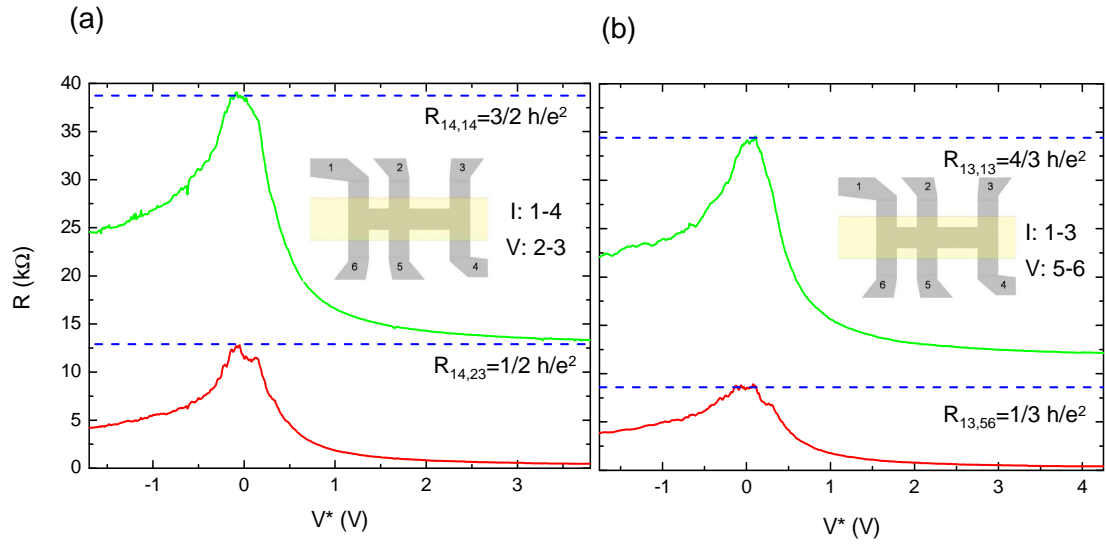


Fig. 3. Four- and two-terminal resistance measured on device S3: (a) $R_{14,23}$ (red line) and $R_{14,14}$ (green line) and (b) $R_{13,56}$ (red line) and $R_{13,13}$ (green line). The dotted blue lines indicate the expected resistance value from a Landauer-Büttiker calculation.

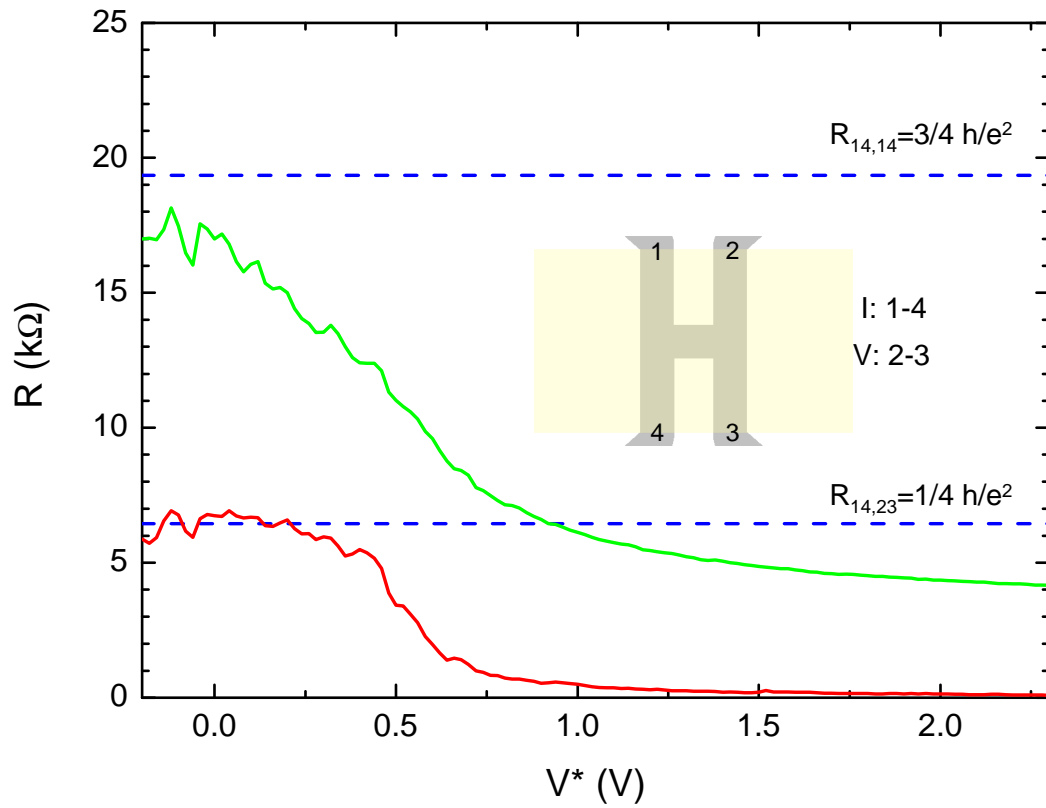


Fig. 4. Nonlocal four-terminal resistance and two-terminal resistance measured on the H-bar device S4: $R_{14,23}$ (red line) and $R_{14,14}$ (green line). Again, the dotted blue line represents the theoretically expected resistance value.